American Mineralogist, Volume 93, pages 426–437, 2008

Crystal chemistry of phlogopite from Vulture-S. Michele Subsynthem volcanic rocks (Mt. Vulture, Italy) and volcanological implications

Silvia Matarrese,[1] Emanuela Schingaro,[1] Fernando Scordari,[1,*] Francesco Stoppa,[2] Gianluigi Rosatelli,[2] Giuseppe Pedrazzi,[3] and Luisa Ottolini[4]

[1]Dipartimento Geomineralogico, Università degli Studi di Bari, via E. Orabona 4, I-70125 Bari, Italy
[2]Dipartimento di Scienze della Terra, Università G.d'Annunzio, via dei Vestini, 3, I-66100 Chieti, Italy
[3]Dipartimento di Sanita' Pubblica, Sezione di Fisica, Plesso Biotecnologico Integrato, via Volturno 39, I-43100, Parma, Italy
[4]CNR-Istituto di Geoscienze e Georisorse (IGG), Sezione di Pavia, via Ferrata, 1, I-27100 Pavia, Italy

Abstract

Volcanic activity at Mt. Vulture lasted about 750 ka and produced SiO_2-undersaturated volcanic rocks that can be classified as old (~700 ka), intermediate (~600–550 ka), and young (~130 ka). The intermediate deposits consist of pyroclastic falls and flows and lavas with compositions ranging from phonolite to foidite. A recent revision of the stratigraphic setting allowed these deposits to be classified into one synthem (the Barile Synthem) and further subdivided into four subsynthems (Toppo S. Paolo, Rionero, Vulture-S. Michele, and Ventaruolo). In the present investigation, trioctahedral micas from sample VUT191 in the Vulture-S. Michele Subsynthem are considered. The host rock has modal diopside (20.2%), analcime (22.8%), plagioclase (27.8%), haüyne (5%), phlogopite (8.9%), and magnetite (6.3%). The micas were studied using chemical (EPMA, C-H-N, SIMS), structural (SCXRD), and spectroscopic (Mössbauer) methods.

EPMA of 36 crystals from thin sections and 6 discrete crystals selected for the structural analysis showed remarkable compositional variability, as follows (in wt%): SiO_2 = 33.14–38.01, Al_2O_3 = 15.56–20.45, MgO = 13.02–20.81, FeO_{tot} = 6.34–14.08, TiO_2 = 2.34–6.02, K_2O = 6.03–9.48, Na_2O = 0.50–0.78, and BaO = 0.89–4.06; all crystals proved to be phlogopite. Elemental C-H-N analyses yielded $H_2O = 2.86 \pm 0.36$ wt%. The water content was also determined by SIMS on two single crystals, labeled VUT191_2 and VUT191_19, which yielded values of 3.81 ± 0.12 and 1.72 ± 0.08 wt% H_2O, respectively. Mössbauer investigation showed that all the iron in VUT191 mica is octahedral with Fe^{2+} = 25.5% and Fe^{3+} = 74.5%, confirming that Vulture micas are particularly Fe^{3+}-rich, as also found from previous investigations. Structure refinements using anisotropic displacement parameters were performed in space group *C*2/*m* and converged at $1.89 \leq R \leq 3.17$, $2.09 \leq R_w \leq 3.43$%. All of the analyzed micas belong to the 1*M* polytype but exhibit remarkable variations in the *c* parameter from 10.1569(4) to 10.2458(4) Å. The chemical and structural parameters indicate that the studied micas can be divided into two groups: the first encompassing strongly dehydrogenated micas affected mainly by Ti-oxy [$^{VI}M^{2+} + 2(OH)^- \leftrightarrow {}^{VI}Ti^{4+} + 2O^{2-} + H_2$] and M^{3+}-oxy [$^{VI}M^{2+} + (OH)^- \leftrightarrow {}^{VI}M^{3+} + O^{2-} + \frac{1}{2}H_2$, with $M^{3+} = Fe^{3+}, Al^{3+}$] substitutions. The second group consist of samples in which vacancy-bearing mechanisms, $2\ {}^{VI}M^{2+} \leftrightarrow {}^{VI}Ti^{4+} + {}^{VI}\square$ and $3\ {}^{VI}M^{2+} \leftrightarrow 2\ {}^{VI}M^{3+} + {}^{VI}\square$ occur.

Keywords: Volcanic phlogopite, Mössbauer spectroscopy, structure refinement, CHN, SIMS, crystal chemistry, substitution mechanisms

Introduction

Phlogopite and biotite are common phases in many volcanic rocks, including andesites, dacites, and rhyolites, as well as potassic and ultrapotassic varieties such as phonolite, foidites, lamprophyres, and lamproites. In principle, these minerals can be used to infer pre-eruptive magmatic conditions, provided that complete chemical analysis, including Fe^{3+}, Fe^{2+}, and H_2O contents, are available. In addition, mica is an important scavenger of some lithophile elements (LILE) (such as Ba) and high-field strength elements (HFSE) (Ti) that are particular soluble in high K, OH^-, and CO_2 melts (Chakmouradian 2006). LILE/HFSE and HFSE concentration/dilution relationships are considered crucial in petrological investigations and magma tectonic assignments. In practice, volcanic micas may undergo complex geologic histories and non-equilibrium conditions. This makes it more difficult to develop activity-composition models for solid solutions in volcanic micas as are needed to determine magmatic intensive variables (Feldstein et al. 1996). In addition, the possibility that the structures and crystal chemistry of micas may preserve a record of the geologic processes they underwent has often been neglected in the past. Only in recent works has the

* E-mail: f.scordari@geomin.uniba.it

crystallographic approach been systematically adopted in the study of geologically well-characterized volcanic micas (Brigatti et al. 2005; Scordari et al. 2006; Matarrese et al. 2006a, 2006b; Matarrese 2007). In contrast, the relationship between crystal chemistry and petrogenesis for metamorphic biotites has been well assessed (Henry and Guidotti et al. 2002; Henry et al. 2005; Cesare et al. 2003).

It is known that understanding the crystal chemistry and solid solution of natural micas is quite a challenge because these minerals are affected by multiple cationic and anionic substitutions. Not only does the chemical disorder involve the tetrahedral (Si, Al, Fe, Ti), octahedral (Mg, Mn, Fe^{2+}, Fe^{3+}, Ti, Al, Cr, □), interlayer (K, Ba, Ca, Na, NH_4, □), and anion (OH^-, O^{2-}, Cl^-, F^-) sites, but the same chemical constituents may enter the mica structure according to different heterovalent substitutions. For example, the most likely mechanisms of Ti substitution are (1) $2\ ^{VI}M^{2+} \leftrightarrow\ ^{VI}Ti^{4+} +\ ^{VI}□$, known as Ti-vacancy (Forbes and Flower 1974); (2) $^{VI}M^{2+} +2\ ^{IV}Si^{4+} \leftrightarrow\ ^{VI}Ti^{4+} +2\ ^{IV}Al^{3+}$, known as Ti-Tschermak (Robert 1976); and (3) $^{VI}M^{2+} + 2(OH)^- \leftrightarrow\ ^{VI}Ti^{4+} + 2O^{2-} + H_2$, known as Ti-oxy (Bohlen et al. 1980).

Different authors have ascertained that Fe^{3+}-oxy [$^{VI}M^{2+} + (OH)^- \leftrightarrow\ ^{VI}Fe^{3+} + O^{2-} + ½H_2$] and Ti-oxy substitutions (mechanism 3 above) play a major role both in metamorphic and igneous phlogopites (Virgo and Popp 2000; Righter et al. 2002; Cesare et al. 2003).

The synergy of several independent analytical techniques is required to correctly assess the substitution mechanisms and correct site populations that form the basis from which reliable activity-composition models may be developed. In the present study, the combination of electron probe micro analysis (EPMA), secondary ion mass spectrometry (SIMS), C-H-N analysis, structural (single-crystal X-ray diffraction, SCXRD), and spectroscopic (Mössbauer) analyses has been used to understand the crystal chemistry of trioctahedral micas from foiditic-phonolitic pyroclastics of Monte Vulture (Potenza, Italy).

The explosive-effusive activity of Mt. Vulture lasted about 750 ka and produced a large variety of alkaline, SiO_2-undersaturated volcanic rocks ranging from carbonatites and melilitites, to foidite, phonolitic-foidite, tephritic-phonolite, and phonolites (Stoppa et al. 2006). Based on their ages (Brocchini et al. 1994), the Vulture products may be classified as old (~700 ka), intermediate (~600–550 ka), and young (~130 ka). Micas are ubiquitous in Mt. Vulture volcanic rocks. According to a recent revision of the stratigraphic setting (Giannandrea et al. 2006) based on Unconformity Bounded Stratigraphic Units (UBSU, Salvador 1987), the intermediate deposits in the central edifice of Monte Vulture consist of four subsynthems (Toppo S. Paolo, Rionero, Vulture-S. Michele, and Ventaruolo) formed by pyroclastic fall and flows and lava products. The four subsynthems are clustered together into the Barile Synthem. The present investigation is focused on the crystal chemistry of trioctahedral micas belonging to this synthem and in particular, originating in the pyroclastic flow deposits, dated 601 ± 7 to 629.6 ± 4.7 ka (Brocchini et al. 1994), belonging to Vulture-S. Michele Subsynthem. The ultimate aim of the investigations on the Mt. Vulture micas is to gain insights into the chemical and structural responses of these minerals to the geologic history of the host rocks.

Materials and methods

The micas of the present work were separated from sample VUT191, which represents the juvenile fraction of the Masseria Saraceno pyroclastic flow, Vulture-San Michele Subsynthem. Micas were given the same label as their host rock. The mode of the phenocrysts in the host rock is 20.2% clinopyroxene, 22.8% analcime, 5.0% haüyne, 8.9% mica, 27.8% plagioclase, 6.3% magnetite, 2.5% apatite, and 5.0% others. The rock name should therefore be pheno-tephrite. However, the presence of a very fine-grained matrix and glass suggests discontinuing pheno-modal classification. The fresh, porphyritic-microcrystalline lava, VUT193, associated with the Masseria Saraceno pyroclastic flow, has a mode of 18.8% diopside, 5.8% leucite, 2.4% K-feldspar, 34.4% anorthoclase, 10.1% haüyne, 8% phlogopite, 6.5% nepheline, and 12.7% plagioclase, along with accessory minerals such as apatite and spinel (<1% each). It is a tephri-phonolite (see Stoppa et al. 2006 for more details). The subhedral mica in VUT191 is not fractured. It contains apatite inclusions and does not show notable deformation features.

Mica separates were obtained by electrostatic separation followed by hand picking. The purity of the concentrates was estimated optically by a reflection microscope to be 99%.

EPMA

Major-elements compositions were determined on 36 crystals from polished thin sections and on six discrete crystals selected from the concentrates and embedded in epoxy resin. The latter crystals were also used for structural analysis.

Chemical compositions of samples in thin sections were measured with a Cameca SX50 in full WDS mode. Analyses were performed at the Natural History Museum (EMMA facilities) of London. Operating conditions were 15 kV, ~20 nA, and 5 µm beam diameter. The standards used were jadeite (Na, Si), periclase (Mg), wollastonite (Ca), rutile (Ti), aluminum oxide (Al), iron oxide (Fe), potassium bromide (K), barium fluoride (Ba), rubidium manganese fluoride (F), halite (Cl), nickel metal (Ni), cromite (Cr), manganese metal (Mn), apatite (P), and celestine (Sr).

The compositions of the six single crystals that were used for structure refinement were measured by wavelength-dispersive spectrometry using a Cameca SX-50 electron microprobe at the Istituto di Geologia Ambientale e Geoingegneria, CNR, Rome, with the following operating conditions: 15 kV accelerating voltage, 15 nA specimen beam current, and 10 µm beam diameter. The following standards were employed: jadeite (Na), periclase (Mg), wollastonite (Si and Ca), rutile (Ti), corundum (Al), magnetite (Fe), orthoclase (K), barite (Ba), fluor-phlogopite (F), sylvite (Cl). A conversion from X-ray counts to oxide weight percentages (wt%) was made with the PAP procedure (Pouchou and Pichoir 1985).

The chemical composition of sample VUT191 bulk rock was determined by multi-method analysis (combination of X-ray Fluorescence, Titration, Atomic Absorption Spectrometry) at the SGS Canada INC Mineral Services, Toronto.

C-H-N

Bulk C, H, and N analysis of mica concentrates was performed with the EA 1108 elemental analyser of CE Instruments at CNR-IGG, Padova, calibrated with standard Acetanilide (C_8H_9NO). The analysis was carried out on ~30 mg of powdered sample.

SIMS

SIMS measurements were performed with a CAMECA IMS 4f ion microprobe installed at the CNR-IGG at Pavia, Italy. A –12.5 kV accelerated $^{16}O^-$ primary ion beam was used having a current intensity of 3–7 nA and a diameter of <5–10 µm beam, following procedures similar to those adopted by L.O. in the paper by Mesto et al. (2006). Sample mounts and standards were left to de-gas overnight in the ion-microprobe sample chamber. Secondary ion signals of the following isotopes were monitored at the electron multiplier: $^1H^+$, $^7Li^+$, $^{19}F^+$, and $^{30}Si^+$ (the latter was used as an inner reference for the matrix). Acquisition times were 20 s (H), 10 s (Li), 50 s (F), and 15 s (Si) over 5 analytical cycles. Detection of positive secondary ions having kinetic energies in the range of 75–125 eV was obtained under steady-state sputtering conditions after 15 min of pre-sputtering. According to previous SIMS work on light elements in silicates, the analysis of "filtered" secondary ions is useful in reducing most chemical matrix effects and in improving the overall measurement reproducibility (Ottolini et al. 1993, 1995 and references therein). Several medium-silica silicate standards were employed for the quantification of the ion signals for H, Li, and F: Finero phlogopite (SiO_2 = 40.04 wt%, 4.20 wt% H_2O, 712 ppm F), kornerupine no.6, schorl no.16, dravite

no.18, and elbaite no.19 (from Ottolini et al. 2002). In particular, we adopted empirical corrections to the ion yield (IY) (H/Si) to consider the variation of the ion signals with increasing (Fe + Mn) content in the sample, as fully described in Ottolini and Hawthorne (2001) and Ottolini et al. (2002). The sample mounts were then re-polished smoothly, carbon coated, and investigated with the electron microprobe proximal to the SIMS craters. These EMPA data were then used in the final SIMS quantification procedures.

Mössbauer spectroscopy

The sample for Mössbauer investigation was prepared by crushing the mica under acetone to minimize atmospheric oxidation and the powdered material was dispersed in a 0.5 inch diameter holder. Transmission ^{57}Fe Mössbauer spectra were obtained on 20 mg of powdered sample at room temperature (RT) using a ^{57}Co thin source in a Rh matrix. The transducer was employed in constant acceleration mode over a Doppler velocity range of ±4 mm/s. Data were acquired on 512 channels and folded to give a flat background and a zero velocity position corresponding to the center shift (CS, also called isomer shift) of metallic α-Fe at RT. The spectrum was fitted using the Voigt-based Quadrupole Splitting Distribution (QSD) method developed by Rancourt and Ping (1991) and implemented in the software RECOIL (Lagarec and Rancourt 1997, 1998). This method assumes that the QSD for each generalized site is composed of a number (*N*) of Gaussian components. The number of Gaussian components is chosen on statistical grounds and has no particular crystal-chemical meaning, but has to ensure that the true QSD of the spectral contribution is well-represented by the sum of Gaussians (Rancourt et al. 1994a, 1994b).

SCXRD

X-ray diffraction (XRD) data were collected from single crystals selected from the mica concentrates, using a Bruker AXS X8 APEX II CCD automated diffractometer equipped with a four-circle Kappa goniometer and graphite-monochromatized Mo*K*α radiation (50 kV and 30 mA operating conditions). Several sets of frames were recorded with a crystal-to-detector distance of 40 mm and a strategy optimized by the APEX suite program (Bruker 2003b). A set of 12 frames was used for initial cell determination, whereas complete data collection was accomplished by several ϕ and ω scans with 0.5° rotation and 10 s exposure time per frame. The whole Ewald sphere (±*h*, ±*k*, ±*l*) was recorded in θ ranges up to ~40°. Reflection intensities were extracted and corrected for Lorentz-polarization using the SAINT program (Bruker 2003a). Absorption correction was applied using SADABS (Sheldrick 2003). Least-squares refinements were performed using the program CRYSTALS (Betteridge et al. 2003) in the space group *C*2/*m*. Starting atomic coordinates were taken from Mesto et al. (2006). The refined parameters were scale factors, atomic positions, cation occupancy factors, and anisotropic displacement parameters. Ionized X-ray scattering curves were employed for non-tetrahedral cations, whereas ionized vs. neutral species were used for Si and O (Hawthorne et al. 1995). At octahedral sites, the electron density was fitted by varying Fe^{2+} vs. Mg^{2+} occupancies with full occupancy constraints, whereas for interlayer and tetrahedral sites, the use of restraints (Watkin 1994) allowed the occupancy to assume values greater than or less than 1. This procedure accounts for interlayer and tetrahedral substitutions and provides a better fit to the electron density, particularly at tetrahedral sites.

Results and discussion

Chemical analyses

Bulk-rock analysis. The chemical composition of sample VUT191 bulk rock is (in oxide wt%): 48.07% SiO_2, 1.04% TiO_2, 18.15% Al_2O_3, 4.24% Fe_2O_3, 3.09% FeO, 0.21% MnO, 4.54% MgO, 9.51% CaO, 4.38% Na_2O, 1.07% K_2O, 0.94% P_2O_5, and 3.91% loss on ignition (L.O.I), with a sum of 99.15%. Sample VUT191 is thus an SiO_2-undersaturated, CaO-rich, alkaline rock with a sodic character having $Na_2O > K_2O$ (Irvine and Bargar 1971). Its high X_{Mg} [X_{Mg} = Mg/(Mg + Fe) ~72] indicates that it is still a primitive rock. High L.O.I. prevents the use of the TAS diagram, but according to the De La Roche diagram (De La Roche et al. 1980), the rock is a "trachy-basalt" that clearly contrasts with its pheno-crystals modal content and associated rocks. Inconsistent chemical classification is explained by the remarkable content of analcime that may replace foids. The associated lava VUT193 is chemically a phonolitic-tephrite (according de La Roche's R1-R2 diagram). Its modal composition is tephritic-phonolite, and may represent an evolved rock derived from VUT191. Thus, the VUT 191 rock sample may be related to a relatively primitive liquid (tephri-foidite) that was able to evolve in composition toward tephritic-phonolitc, possibly through clinopyroxene crystal settling in a magma chamber and an increase in feldspar content.

Micas analyses. The results of electron microprobe analysis are reported on Table 1 for micas from thin section and in Tables 2 and 3, for mica single crystals that were used structure refinement. The latter analyses represent averages of 5–10 spots per crystal. Considering the whole data set, VUT191 phlogopite is characterized by remarkable chemical inhomogeneity, as revealed by the generally large ranges in oxide wt%: 33.14–38.01 for SiO_2, 15.56–20.45 for Al_2O_3, 13.02–20.81 for MgO, 6.34–4.08 for FeO_{tot}, 2.34–6.02 for TiO_2, 6.03–9.48 for K_2O, 0.50–0.78 for Na_2O, and 0.89–4.06 for BaO.

The H_2O content determined from C-H-N analysis is 2.86 ± 0.36 wt%. This value is the average of two different measurements (that yielded 3.11 and 2.60 wt%) performed on different aliquots of the same mica sample. This result suggests a degree of inhomogeneity of OH concentration, which also has been documented for other Mt. Vulture phlogopites (Mesto et al. 2006). No nitrogen was detected in the analyzed samples, whereas the carbon content was 0.18 ± 0.02 wt% C.

SIMS measurements were performed on two out of the six single crystals used for structure refinement (VUT191_2 and VUT191_19), selected on the basis of their different chemistries and *c*-parameters (see below). The grain to grain chemical variability noted above extends to light elements (H, Li, F, see Tables 2 and 3).

All considered, the analyzed samples are solid solutions between phlogopite [$KMg_3AlSi_3O_{10}(OH)_2$] and annite [$KFe^{2+}_3AlSi_3O_{10}(OH)_2$] with Ti 0.10–0.38 apfu, Ba 0.03–0.12 apfu, and a variable degree of dehydrogenation. The atomic ratios for data from single crystals, as listed in Table 3, were calculated on the basis on 12(O, OH, Cl, F), assuming all Ti as Ti^{4+} and using the Fe^{2+}/Fe^{3+} ratios provided by the Mössbauer investigation (see below). Final crystal-chemical formulae and a critical discussion of data in Table 3 are postponed to the section on crystal chemistry below.

Figure 1 is a plot of the annite component [$Fe_{tot}/(Fe_{tot} + Mg)$], vs. the Ti content (apfu) for the samples of the present study. For comparison, data from other well-characterized micas from Mt. Vulture, all from the Barile Synthem but from different subsynthems, are also shown. Unlike micas belonging to other subsynthems (such as SA sample, from Rionero Subsynthem as discussed in Scordari et al. 2006) and the VUT187 sample from the Ventaruolo Subsynthem, the VUT191 phlogopite has an annite component that spans almost the whole interval of variation (0.15–0.40) found so far for Monte Vulture micas (Matarrese et al. 2006, 2007).

Mössbauer spectroscopy

The results of the Mössbauer investigation are reported in Table 4 and typical Mössbauer spectra of the micas are displayed in Figure 2. Three absorption bands occur at approximately –0.2,

TABLE 1. Electron microprobe data (wt%) for VUT191 phlogopites in thin sections

Sample	191_1	191_3	191_4	191_5	191_6	191_7	191_8	191_9	191_10	191_12	191_14	191_15	191_16	191_17
SiO_2	37.416	36.616	35.596	33.848	33.574	34.105	33.805	36.706	36.868	37.459	34.291	33.257	33.138	36.293
Al_2O_3	17.207	17.430	16.808	15.767	15.909	15.883	15.898	16.606	17.713	16.801	16.308	15.690	15.563	17.534
MgO	19.623	18.148	15.619	14.556	14.550	14.818	14.445	20.219	18.889	19.872	14.369	14.065	13.434	18.149
FeO_{tot}	6.337	8.268	12.133	12.835	12.525	12.864	12.960	7.649	7.432	6.917	12.954	12.997	13.445	8.392
TiO_2	2.344	3.022	3.876	5.721	5.539	5.464	5.816	2.891	2.585	2.539	5.503	6.022	5.706	2.951
Cr_2O_3	0.140	0.000	0.000	0.000	0.000	0.000	0.000	0.092	0.023	0.067	0.026	0.007	0.018	0.094
MnO	0.017	0.035	0.179	0.231	0.245	0.192	0.152	0.037	0.022	0.045	0.205	0.178	0.209	0.070
K_2O	9.009	8.760	9.154	8.298	8.201	8.357	8.155	9.404	8.916	9.140	8.772	8.014	7.417	8.819
Na_2O	0.538	0.656	0.594	0.569	0.597	0.567	0.541	0.604	0.613	0.603	0.569	0.527	0.677	0.616
BaO	0.909	1.207	1.278	3.680	3.520	3.306	3.564	1.106	0.933	0.972	1.459	4.058	3.472	1.282
CaO	0.194	0.115	0.050	0.038	0.057	0.069	0.105	0.127	0.206	0.173	0.137	0.153	0.554	0.081
F	n.d.	n.d.	n.d.	n.d.	n.d.	n.d.	n.d.	n.d.	n.d.	n.d.	n.d.	n.d.	n.d.	n.d.
Cl	0.039	0.016	0.072	0.136	0.112	0.076	0.098	0.017	0.023	0.027	0.095	0.103	0.094	0.040
Sum	94.30	94.96	96.367	96.745	95.86	96.77	96.616	96.106	94.893	95.19	95.764	96.151	94.844	95.018
FeO*	1.606	2.096	3.076	3.254	3.175	3.261	3.285	1.939	1.884	1.753	3.284	3.295	3.408	2.127
Fe_2O_3*	5.257	6.859	10.065	10.648	10.391	10.672	10.751	6.345	6.165	5.738	10.746	10.782	11.154	6.962

	191_19	191_20	191_21	191_22	191_23	191_24	191_25	191_26	191_27	191_28	191_29	191_30	191_33	191_34
SiO_2	38.011	36.438	36.862	34.549	34.400	33.950	34.697	33.655	33.236	37.061	36.188	33.884	35.831	33.465
Al_2O_3	20.447	16.982	18.052	16.147	16.109	15.820	16.109	15.792	15.741	17.931	17.679	16.408	17.230	15.888
MgO	15.619	19.240	18.124	14.914	14.385	14.240	15.025	14.775	14.666	18.101	14.513	13.021	16.251	14.438
FeO_{tot}	7.827	7.791	8.048	12.918	12.709	12.696	12.313	12.723	12.927	8.268	13.005	14.079	11.958	12.435
TiO_2	2.560	3.148	2.969	5.449	5.671	5.650	5.186	6.003	5.548	2.981	3.413	5.308	3.119	5.608
Cr_2O_3	0.012	0.051	0.000	0.000	0.042	0.032	0.000	0.000	0.000	0.060	0.070	0.063	0.000	0.037
MnO	0.050	0.065	0.077	0.213	0.199	0.141	0.124	0.244	0.196	0.077	0.230	0.287	0.170	0.189
K_2O	7.477	8.999	8.642	8.862	8.121	8.336	8.742	8.112	8.313	8.542	6.033	8.245	8.944	8.156
Na_2O	0.569	0.656	0.660	0.549	0.519	0.572	0.539	0.589	0.543	0.582	0.783	0.499	0.534	0.530
BaO	1.073	1.242	1.284	2.039	3.228	3.343	1.901	3.873	3.176	1.310	0.888	2.981	1.124	3.309
CaO	0.189	0.071	0.118	0.077	0.108	0.113	0.095	0.143	0.162	0.164	2.332	0.090	0.144	0.078
F	n.d	n.d	n.d	n.d	n.d	n.d	n.d	n.d	n.d	n.d	n.d	n.d	n.d	n.d
Cl	0.027	0.060	0.028	0.097	0.107	0.100	0.104	0.090	0.091	0.037	0.086	0.079	0.087	0.097
Sum	94.511	95.39	95.533	96.887	96.654	96.048	95.858	97.056	95.673	95.801	96.301	96.114	96.386	95.236
FeO*	1.984	1.975	2.040	3.275	3.222	3.218	3.121	3.225	3.277	2.096	3.297	3.569	3.031	3.152
Fe_2O_3*	6.493	6.463	6.677	10.717	10.543	10.532	10.215	10.555	10.724	6.859	10.789	11.680	9.920	10.316

	191_35	191_36	191_37	191_38	191_39	191_40	191_204	191_214
SiO_2	35.630	33.568	33.991	36.511	36.607	36.552	34.845	37.331
Al_2O_3	16.404	15.858	16.088	16.682	16.612	16.910	15.801	17.007
MgO	17.834	14.765	14.243	20.663	20.810	18.754	15.526	19.976
FeO_{tot}	11.098	13.379	13.210	6.632	6.760	7.725	12.542	8.367
TiO_2	3.099	5.226	5.406	2.804	2.809	3.049	4.435	3.238
Cr_2O_3	0.004	0.000	0.000	0.056	0.000	0.009	0.000	0.091
MnO	0.129	0.213	0.201	0.090	0.084	0.008	0.183	0.059
K_2O	9.298	8.634	8.318	9.217	9.411	9.028	9.480	9.119
Na_2O	0.543	0.566	0.554	0.567	0.578	0.600	0.576	0.581
BaO	1.163	3.207	3.281	1.154	1.185	1.351		
CaO	0.067	0.050	0.067	0.084	0.087	0.119	0.013	0.067
F	n.d.	n.d.	n.d.	n.d.	n.d.	n.d	n.d	n.d
Cl	0.049	0.111	0.087	0.064	0.027	0.037	0.050	0.010
Sum	96.24	96.689	96.544	95.075	95.532	94.784	94.493	96.541
FeO*	2.813	3.392	3.349	1.681	1.714	1.958	3.179	2.121
Fe_2O_3*	9.207	11.099	10.959	5.502	5.608	6.409	10.405	6.941

Note: n.d. = not determined.
* From Mössbauer spectroscopy.

1.0, and 2.3 mm/s that correspond respectively to (1) the sum of low-energy lines of $^{VI}Fe^{2+}$ and $^{VI}Fe^{3+}$ doublets; (2) the high-energy line of the $^{VI}Fe^{3+}$ doublet; and (3) the high-energy component of the $^{VI}Fe^{2+}$ doublet. No shoulder at ~0.5 mm/s (which would be evidence for the occurrence of tetrahedral Fe^{3+}; see Redhammer et al. 2005) was observed. In Table 4, the results of n_1-n_2 fittings are compiled, where n_1 and n_2 are the numbers of assumed QSD Gaussian components for $^{VI}Fe^{2+}$ $^{VI}Fe^{3+}$ sites, respectively. For the sample analyzed here, $n_1 = n_2 = 1$. A^-/A^+ ratios were allowed to vary during fitting (see Table 4) to account for the possibility that the orientation of crystallites in the analyzed powder is not completely random (Rancourt et al. 1994b).

The fitting parameters are consistent with those reported in the literature for synthetic and natural trioctahedral micas (Redhammer 1998; Rancourt et al. 1993, 1994a; Shabani 1999; Dyar 2002, Redhammer et al. 2005). The sample is Fe^{3+}-rich, having $Fe^{2+} \approx 25\%$ and $Fe^{3+} \approx 75\%$.

Previous investigations have shown that Mt. Vulture micas are characterized by a variable but nevertheless high ratio of Fe^{3+}/Fe_{tot}, ranging from 42 to 88% (Matarrese et al. 2005, 2006, 2007; Scordari et al. 2006; Schingaro et al. 2006; Matarrese 2007). Focusing only on micas from intermediate Vulture volcanics, Scordari et al. (2006) have found 44% Fe^{2+} and 56% Fe^{3+} in their SA sample (Rionero Subsynthem), whereas Schingaro et al. (in review) studied a phlogopite from the Ventaruolo Subsynthem that has 13% Fe^{2+} and 87% Fe^{3+}. However, the typical Fe^{3+}/Fe_{tot} for Mt. Vulture micas is ~50% (Matarrese 2007), and in all cases where an Fe^{3+}/Fe_{tot} ratio >> 50% has been found, late- and/or post-magmatic events can be invoked, which affected the original Fe^{3+} contents.

TABLE 2. Average electron microprobe data (wt%) for VUT191 single crystals used for structure refinement

Sample name	VUT191 _1	VUT191 _2	VUT191 _10	VUT191 _11	VUT 191 _13	VUT191 _19
SiO_2	37.036	37.198	33.600	33.980	35.078	34.360
Al_2O_3	17.098	16.354	15.879	15.730	16.343	15.969
MgO	20.238	19.404	15.586	14.716	14.677	14.699
FeO_{tot}	6.620	6.800	11.599	11.682	11.696	12.214
TiO_2	2.405	2.640	4.623	4.654	4.579	5.063
Cr_2O_3	0.147	0.053	0.007	0.003	0.011	0.007
MnO	0.046	0.042	0.124	0.178	0.210	0.175
NiO	0.022	0.041	0.015	0.028	0.025	0.020
Li_2O	–	0.009	–	–	–	0.027
K_2O	8.488	8.749	8.088	7.749	7.851	7.877
Na_2O	0.608	0.600	0.592	0.599	0.631	0.565
BaO	1.035	0.971	2.398	2.976	2.474	2.836
CaO	0.011	0.012	0.026	0.075	0.033	0.021
F	0.415	0.640‡	0.621	0.945	0.884	1.280‡
Cl	0.024	0.037	0.084	0.088	0.111	0.09
H_2O	2.860†	3.810‡	2.86†	2.86†	2.86†	1.720‡
Total	97.683	96.461	95.947	95.635	96.865	95.829
FeO*	1.678	1.718	2.940	2.979	2.982	3.115
Fe_2O_3*	5.492	5.622	9.623	8.703	9.683	10.112

* Mössbauer results used to recast FeO_{tot} into FeO and Fe_2O_3.
† Average value from C-H-N analysis (see text).
‡ From SIMS.

TABLE 3. Atomic proportions (apfu) as determined from data in Table 2

Sample name	VUT 191 _1	VUT 191 _2	VUT191 _10	VUT191 _11	VUT191 _13	VUT191 _19
Si	2.735	2.715	2.584	2.632	2.652	2.658
^{IV}Al	1.265	1.285	1.368	1.294	1.348	1.342
Σ T	4.000	4.000	4.000	4.000	4.000	4.000
^{VI}Al	0.223	0.122	0.068	0.182	0.108	0.114
Mg	2.228	2.112	1.699	1.747	1.654	1.695
Fe^{+2}	0.104	0.105	0.193	0.197	0.189	0.202
Fe^{+3}	0.305	0.310	0.507	0.581	0.551	0.589
Ti	0.134	0.145	0.271	0.279	0.260	0.295
Cr	0.019	0.007	0.000	0.000	0.001	0.001
Mn	0.003	0.003	0.012	0.012	0.001	0.011
Ni	0.001	0.002	0.001	0.002	0.002	0.001
Li	–	0.003	–	–	–	0.008
Σ Oct	3.015	2.809	2.832	2.751	2.764	2.916
K	0.800	0.815	0.766	0.787	0.757	0.777
Na	0.087	0.085	0.090	0.093	0.092	0.085
Ba	0.030	0.028	0.090	0.093	0.073	0.086
Ca	0.001	0.001	0.000	0.006	0.003	0.002
Σ I	0.917	0.927	0.946	0.979	0.923	0.948
OH^-	1.410	1.857	1.479	0.670	1.443	0.888
F	0.097	0.148	0.232	0.238	0.211	0.313
Cl	0.003	0.005	0.012	0.012	0.014	0.012
O	0.490	0.000	0.278	1.080	0.331	0.787

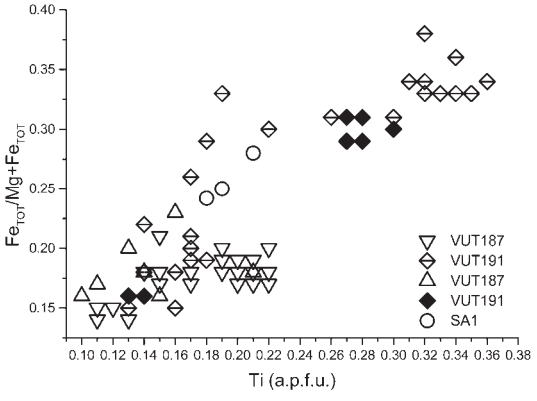

FIGURE 1. A plot of Fe/(Fe + Mg), thought to represent the amount of the annite component vs. Ti content for micas from Monte Vulture intermediate pyroclastics (Barile Synthem). Diamonds = Barred symbols are VUT191 phlogopites from thin section, this work; full symbols are single crystals of VUT191 phlogopite, this work; open triangles = VUT187 phlogopite, Schingaro et al. (in review); open circles = SA1 phlogopite single crystals data from Scordari et al. (2006).

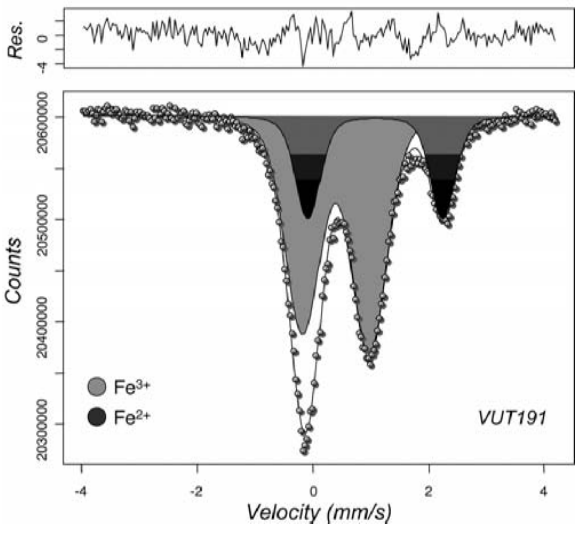

FIGURE 2. Room-temperature Mössbauer spectrum of VUT191 phlogopite.

Structural features

Details on data collection, lattice parameters, results of structure refinements, fractional atomic coordinates, partial occupancies, anisotropic, and equivalent isotropic refinements are given in Tables 5 and 6. Tables 7 and 8 contain selected bond lengths and distortion parameters describing the polyhedral and layer geometry for the studied samples. Atomic labeling is the same as in Hazen and Burnham (1973). The refinements performed in space group $C2/m$ converged at $1.89 \le R \le 3.17$, $2.09 \le R_w \le 3.43\%$. The difference Fourier maps revealed hydrogen in the expected position for all samples, but extra peaks were observed for samples VUT191_10 and VUT191_11. In particular for sample VUT191_10, the initial structure refinement converged at $R = 7.49$, $R_w = 7.88\%$ and the residual electron density gave $\rho_{min} = -0.75$, and $\rho_{max} = 7.24$ e$^-$/Å^3. The same parameters for sample VUT191_11 were $R = 4.30$, $R_w = 4.75\%$, $\rho_{min} = -0.45$, and $\rho_{max} = 2.68$ e–/Å^3. Extra peaks in difference Fourier syntheses apparently pointed to $\pm b/3$ shifts of the T and K atomic positions (Schingaro et al. 2001). It turned out that these samples were affected by the Ďurovič effect (Nespolo and Ferraris 2001), so that the large residues in electron density maps could be ascribed to systematic wrong measurements of non-family reflections. In subsequent refinements, different scales were allowed to vary for reflections hkl with $k = 3n$ and hkl with $k \neq 3n$, which refined to 0.563(1), 0.437(1) and 0.533(1), 0.467(1) for VUT191_10, and VUT191_11, respectively.

TABLE 4. Mössbauer parameters obtained by QSD fitting method

	χ^2	Species	Γ/2 (mm/s)	δ_0* (mm/s)	A^-/A^+	ΔE_Q (mm/s)	σ (mm/s)	P (%)	A (%)
VUT191	1.75	Fe^{2+}	0.097*	1.083(10)	1†	2.333(21)	0.338(16)	100*	25.5(6)
		Fe^{3+}		0.3987(57)	0.9147(89)	1.151(10)	0.5197(82)	100*	74. 5(6)

* $\delta_1 = 0$.
† Fixed value.

TABLE 5. Crystal, experimental, and refinement data for VUT191 phlogopite

	VUT191_1	VUT191_2	VUT191_10	VUT191_11	VUT191_13	VUT191_19
Space group	*C2/m*	*C2/m*	*C2/m*	*C2/m*	*C2/m*	*C2/m*
a (Å)	5.3252(2)	5.3254(4)	5.3380(2)	5.3367(3)	5.3377(2)	5.3341(2)
b (Å)	9.2205(3)	9.2216(7)	9.2430(3)	9.2431(5)	9.2424(4)	9.2387(3)
c (Å)	10.2458(4)	10.2411(9)	10.1923(3)	10.1806(5)	10.1654(4)	10.1569(4)
β (°)	99.9938(26)	100.0223(64)	100.0814(21)	100.1033(42)	100.0990(32)	100.0597(27)
Cell volume (Å³)	495.442	495.255	495.116	494.404	493.721	492.836
Z	2	2	2	2	2	2
Crystal size (mm)	0.17 × 0.31 × 0.03	0.27 × 0.25 × 0.01	0.37 × 0.33 × 0.02	0.22 × 0.29 × 0.02	0.28 × 0.14 × 0.03	0.27 × 0.24 × 0.01
θ range for data collection	2–31°	2–39°	2–36°	2–36°	2–44°	4–36°
Reflections measured /unique	11606/836 [R_{int} = 0.039]	23889/1635 [R_{int} = 0.054]	1257/1257 [R_{int} = 0.053]	1258/1258 [R_{int} = 0.047]	8468/1944 [R_{int} = 0.035]	6972/1256 [R_{int} = 0.031]
Reflections used [$I > 3\sigma(I)$]	438	446	729	517	711	612
No. of refined parameters	71	71	73	73	71	71
Goof*	0.83	0.83	0.43	0.62	0.69	0.75
R_1†	3.17	3.14	1.89	2.33	2.67	2.77
Rw †	3.43	3.29	2.09	2.46	2.94	3.14
$\Delta\rho_{min}$, $\Delta\rho_{max}$ (e/Å³)	–0.21, 0.44	–0.20, 0.41	–0.17, 0.24	–0.21, 0.20	–0.22, 0.29	–0.16, 0.38

* Goodness-of-fit = $[\Sigma[w(F_o^2 - F_c^2)^2]/(N - P)]^{1/2}$. where *N* and *P* are the number of reflections and parameters, respectively.
† $R_1 = \Sigma[|F_o| - |F_c|]/\Sigma|F_o|$; $R_w = [\Sigma[w(|F_o| - |F_c|)^2]/\Sigma w|F_o|^2]^{1/2}$.

TABLE 6. Results of structure refinement in space group *C2/m*: crystallographic coordinates, equivalent isotropic displacement parameters (Å²), partial occupancies and anisotropic displacement parameters

Site	Atom	*x/a*	*y/b*	*z/c*	$U_{iso/equiv}$	Occupancy	U_{11}	U_{22}	U_{33}	U_{23}	U_{13}	U_{12}
VUT191_1												
K	K^+	0.0000	0.0000	0.0000	0.0342	1.0049(9)	0.0328(12)	0.0334(13)	0.0363(14)	0.0000	0.0060(10)	0.0000
M1	Mg^{2+}	0.0000	0.5000	0.5000	0.0123	0.8468(8)	0.0098(11)	0.0077(10)	0.0203(13)	0.0000	0.0052(10)	0.0000
	Fe^{2+}	0.0000	0.5000	0.5000	0.0123	0.1532(7)	0.0098(11)	0.0077(10)	0.0203(13)	0.0000	0.0052(10)	0.0000
M2	Mg^{2+}	0.0000	0.83464(19)	0.5000	0.0138	0.8319(8)	0.0091(7)	0.0127(7)	0.0196(8)	0.0000	0.0029(6)	0.0000
	Fe^{2+}	0.0000	0.83464(19)	0.5000	0.0138	0.1681(8)	0.0091(7)	0.0127(7)	0.0196(8)	0.0000	0.0029(6)	0.0000
T	Si^{4+}	0.57542(19)	0.16675(12)	0.22673(12)	0.0136	0.4137(10)	0.0114(4)	0.0103(4)	0.0193(5)	0.0003(6)	0.0032(4)	0.0000(5)
	Si	0.07542(19)	0.16675(12)	0.22673(12)	0.0136	0.5765(10)	0.0114(4)	0.0103(4)	0.0193(5)	0.0003(6)	0.0032(4)	0.0000(5)
O1	O,O^{2-}	0.8310(6)	0.2255(4)	0.1694(3)	0.0219	1	0.0189(14)	0.0228(16)	0.0245(16)	–0.0032(14)	0.0051(12)	–0.0039(13)
O2	O,O^{2-}	0.5067(8)	0.0000	0.1702(5)	0.0216	1	0.023(2)	0.016(2)	0.025(2)	0.0000	0.0011(18)	0.0000
O3	O,O^{2-}	0.6306(5)	0.1673(3)	0.3908(3)	0.0146	1	0.0112(12)	0.0131(12)	0.0195(14)	–0.0004(14)	0.0027(10)	–0.0003(12)
O4	O,O^{2-}	0.1321(8)	0.0000	0.3992(5)	0.0148	1	0.015(2)	0.014(2)	0.016(2)	0.0000	0.0033(18)	0.0000
	H	0.106(18)	0.0000	0.321(10)	0.0148	0.7607(10)	0.015(2)	0.014(2)	0.016(2)	0.0000	0.0033(18)	0.0000
VUT191_2												
K	K^+	0.0000	0.0000	0.0000	0.0394	1.0188(9)	0.0375(13)	0.0359(13)	0.0454(16)	0.0000	0.0087(11)	0.0000
M1	Mg^{2+}	0.0000	0.5000	0.5000	0.0173	0.8478(8)	0.0136(12)	0.0111(12)	0.0286(16)	0.0000	0.0074(11)	0.0000
	Fe^{2+}	0.0000	0.5000	0.5000	0.0173	0.1521(7)	0.0136(12)	0.0111(12)	0.0286(16)	0.0000	0.0074(11)	0.0000
M2	Mg^{2+}	0.0000	0.8360(2)	0.5000	0.0194	0.8109(8)	0.0135(7)	0.0170(8)	0.0282(10)	0.0000	0.0050(7)	0.0000
	Fe^{2+}	0.0000	0.8360(2)	0.5000	0.0194	0.1891(8)	0.0135(7)	0.0170(8)	0.0282(10)	0.0000	0.0050(7)	0.0000
T	Si^{4+}	0.57527(19)	0.16678(14)	0.22626(12)	0.0180	0.4483(10)	0.0142(4)	0.0127(5)	0.0279(6)	–0.0005(8)	0.0057(4)	–0.0002(6)
	Si	0.57527(19)	0.16678(14)	0.22626(12)	0.0180	0.5479(10)	0.0142(4)	0.0127(5)	0.0279(6)	–0.0005(8)	0.0057(4)	–0.0002(6)
O1	O,O^{2-}	0.8315(6)	0.2245(4)	0.1692(3)	0.0271	1	0.0226(14)	0.0287(18)	0.0315(17)	–0.0032(15)	0.0085(13)	–0.0060(13)
O2	O,O^{2-}	0.5055(9)	0.0000	0.1696(5)	0.0269	1	0.031(3)	0.017(2)	0.031(3)	0.0000	0.002(2)	0.0000
O3	O,O^{2-}	0.6302(5)	0.1675(4)	0.3913(3)	0.0181	1	0.0135(12)	0.0136(13)	0.0280(17)	0.0004(16)	0.0055(11)	0.0002(14)
O4	O,O^{2-}	0.1337(9)	0.0000	0.4006(5)	0.0181	1	0.016(2)	0.015(2)	0.024(3)	0.0000	0.005(2)	0.0000
	H	0.103(15)	0.0000	0.327(6)	0.0181	0.9009(10)	0.016(2)	0.015(2)	0.024(3)	0.0000	0.005(2)	0.0000

In the final step of the anisotropic refinements, the hydrogen atom was added to the model. Its coordinates and occupancy were refined (see Table 6), whereas the displacement parameters were made to ride those of the O4 atom. The final O-H distances were in the range 0.74(6)–0.87(5) Å.

The variation of the *c*-parameter, which ranges from 10.1569(4) Å (sample VUT191_19) to 10.2458(4) Å (sample VUT191_1, see Table 5) is notable. This behavior is peculiar for micas of the Vulture-S. Michele Subsynthem, because in all other subsynthems so far investigated, the relevant phlogopites have much smaller ranges of variation (Matarrese et al. 2006; Schingaro et al. 2006; Matarrese 2007). This feature seems to reflect the grain-to-grain variability of chemical composition already highlighted above. However, the *c* parameters observed for the micas of this study are small when compared with those of close-to-end-member annite [10.3235(4) Å, Redhammer and Roth (2002)] and close-to-end-member phlogopite [10.291(4) Å, Alietti et al. (1995); 10.3100(54) Å, synthetic sample Phl no. 2

TABLE 6. —*CONTINUED*

Site	Atom	*x/a*	*y/b*	*z/c*	$U_{iso/equiv}$	Occupancy	U_{11}	U_{22}	U_{33}	U_{23}	U_{13}	U_{12}
VUT191_10												
K	K^+	0.0000	0.0000	0.0000	0.0292	1.1088(8)	0.0272(4)	0.0277(5)	0.0331(5)	0.0000	0.0061(4)	0.0000
M1	Mg^{2+}	0.0000	0.5000	0.5000	0.0115	0.6593(8)	0.0116(4)	0.0072(4)	0.0163(5)	0.0000	0.0043(3)	0.0000
	Fe^{2+}	0.0000	0.5000	0.5000	0.0115	0.3407(7)	0.0116(4)	0.0072(4)	0.0163(5)	0.0000	0.0043(3)	0.0000
M2	Mg^{2+}	0.0000	0.83813(9)	0.5000	0.0124	0.6424(8)	0.0093(2)	0.0135(3)	0.0142(3)	0.0000	0.00149(19)	0.0000
	Fe^{2+}	0.0000	0.83813(9)	0.5000	0.0124	0.3569(7)	0.0093(2)	0.0135(3)	0.0142(3)	0.0000	0.00149(19)	0.0000
T	Si^{4+}	0.57472(8)	0.16706(7)	0.22445(4)	0.0101	0.2912(9)	0.00869(16)	0.00913(17)	0.01244(18)	–0.0003(3)	0.00202(13)	0.0000(2)
	Si	0.57472(8)	0.16706(7)	0.22445(4)	0.0101	0.7013(9)	0.00869(16)	0.00913(17)	0.01244(18)	–0.0003(3)	0.00202(13)	0.0000(2)
O1	O,O^{2-}	0.8283(3)	0.22651(18)	0.16700(14)	0.0187	1	0.0166(6)	0.0231(7)	0.0170(6)	–0.0028(6)	0.0044(5)	–0.0057(6)
O2	O,O^{2-}	0.5089(4)	0.0000	0.1682(2)	0.0189	1	0.0239(10)	0.0145(9)	0.0169(9)	0.0000	–0.0008(7)	0.0000
O3	O,O^{2-}	0.6307(2)	0.16822(18)	0.39132(13)	0.0118	1	0.0114(5)	0.0109(5)	0.0134(5)	0.0000(6)	0.0023(4)	0.0003(6)
O4	O,O^{2-}	0.1326(4)	0.0000	0.3996(2)	0.0123	1	0.0112(8)	0.0131(9)	0.0125(9)	0.0000	0.0018(7)	0.0000
	H	0.108(9)	0.0000	0.313(5)	0.0123	0.7867(10)	0.0112(8)	0.0131(9)	0.0125(9)	0.0000	0.0018(7)	0.0000
VUT191_11												
K	K^+	0.0000	0.0000	0.0000	0.0298	1.1219(9)	0.0257(7)	0.0268(7)	0.0376(9)	0.0000	0.0074(6)	0.0000
M1	Mg^{2+}	0.0000	0.5000	0.5000	0.0128	0.6897(8)	0.0119(7)	0.0080(7)	0.0195(9)	0.0000	0.0057(6)	0.0000
	Fe^{2+}	0.0000	0.5000	0.5000	0.0128	0.3105(7)	0.0119(7)	0.0080(7)	0.0195(9)	0.0000	0.0057(6)	0.0000
M2	Mg^{2+}	0.0000	0.83933(14)	0.5000	0.0141	0.6458(8)	0.0095(4)	0.0147(5)	0.0182(6)	0.0000	0.0027(4)	0.0000
	Fe^{2+}	0.0000	0.83933(14)	0.5000	0.0141	0.3542(8)	0.0095(4)	0.0147(5)	0.0182(6)	0.0000	0.0027(4)	0.0000
T	Si^{4+}	0.57436(12)	0.16733(11)	0.22395(8)	0.0123	0.5401(10)	0.0094(3)	0.0110(3)	0.0169(4)	0.0002(5)	0.0034(3)	–0.0004(4)
	Si	0.57436(12)	0.16733(11)	0.22395(8)	0.0123	0.4532(10)	0.0094(3)	0.0110(3)	0.0169(4)	0.0002(5)	0.0034(3)	–0.0004(4)
O1	O,O^{2-}	0.8277(4)	0.2269(3)	0.1662(2)	0.0210	1	0.0170(9)	0.0241(12)	0.0226(11)	–0.0033(10)	0.0050(8)	–0.0058(9)
O2	O,O^{2-}	0.5087(6)	0.0000	0.1673(3)	0.0202	1	0.0256(16)	0.0151(14)	0.0186(16)	0.0000	0.0006(12)	0.0000
O3	O,O^{2-}	0.6308(4)	0.1683(3)	0.3915(2)	0.0143	1	0.0129(9)	0.0130(9)	0.0174(10)	0.0005(12)	0.0034(7)	0.0006(10)
O4	O,O^{2-}	0.1331(6)	0.0000	0.4001(4)	0.0137	1	0.0107(14)	0.0154(16)	0.0146(17)	0.0000	0.0014(13)	0.0000
	H	0.092(15)	0.0000	0.321(6)	0.0137	0.6645(10)	0.0107(14)	0.0154(16)	0.0146(17)	0.0000	0.0014(13)	0.0000
VUT191_13												
K	K^+	0.0000	0.0000	0.0000	0.0292	1.1294(9)	0.0251(6)	0.0259(6)	0.0367(8)	0.0000	0.0058(5)	0.0000
M1	Mg^{2+}	0.0000	0.5000	0.5000	0.0107	0.7072(8)	0.0082(6)	0.0078(6)	0.0169(7)	0.0000	0.0045(5)	0.0000
	Fe^{2+}	0.0000	0.5000	0.5000	0.0107	0.2927(7)	0.0082(6)	0.0078(6)	0.0169(7)	0.0000	0.0045(5)	0.0000
M2	Mg^{2+}	0.0000	0.84067(11)	0.5000	0.0129	0.6401(8)	0.0068(3)	0.0159(4)	0.0160(4)	0.0000	0.0017(3)	0.0000
	Fe^{2+}	0.0000	0.84067(11)	0.5000	0.0129	0.3598(8)	0.0068(3)	0.0159(4)	0.0160(4)	0.0000	0.0017(3)	0.0000
T	Si^{4+}	0.57405(12)	0.16701(9)	0.22365(7)	0.0112	0.3577(10)	0.0092(3)	0.0102(3)	0.0141(3)	0.0001(4)	0.0020(2)	–0.0001(3)
	Si	0.57405(12)	0.16701(9)	0.22365(7)	0.0112	0.6352(10)	0.0092(3)	0.0102(3)	0.0141(3)	0.0001(4)	0.0020(2)	–0.0001(3)
O1	O,O^{2-}	0.8267(4)	0.2278(3)	0.1657(2)	0.0202	1	0.0178(9)	0.0247(11)	0.0189(9)	–0.0039(9)	0.0049(7)	–0.0066(8)
O2	O,O^{2-}	0.5103(6)	0.0000	0.1676(3)	0.0207	1	0.0248(15)	0.0136(12)	0.0215(15)	0.0000	–0.0021(12)	0.0000
O3	O,O^{2-}	0.6310(3)	0.1689(2)	0.39121(19)	0.0119	1	0.0106(7)	0.0111(7)	0.0140(8)	–0.0006(8)	0.0018(6)	0.0008(7)
O4	O,O^{2-}	0.1326(6)	0.0000	0.4004(3)	0.0135	1	0.0122(12)	0.0144(13)	0.0143(14)	0.0000	0.0032(11)	0.0000
	H	0.105(14)	0.0000	0.322(8)	0.0135	0.6826(10)	0.0122(12)	0.0144(13)	0.0143(14)	0.0000	0.0032(11)	0.0000
VUT191_19												
K	K^+	0.0000	0.0000	0.0000	0.0287	1.1286(9)	0.0253(7)	0.0245(7)	0.0365(10)	0.0000	0.0061(6)	0.0000
M1	Mg^{2+}	0.0000	0.5000	0.5000	0.0112	0.7150(8)	0.0086(7)	0.0065(6)	0.0192(9)	0.0000	0.0048(6)	0.0000
	Fe^{2+}	0.0000	0.5000	0.5000	0.0112	0.2848(7)	0.0086(7)	0.0065(6)	0.0192(9)	0.0000	0.0048(6)	0.0000
M2	Mg^{2+}	0.0000	0.84109(13)	0.5000	0.0126	0.6459(8)	0.0069(4)	0.0140(5)	0.0169(5)	0.0000	0.0020(4)	0.0000
	Fe^{2+}	0.0000	0.84109(13)	0.5000	0.0126	0.3539(8)	0.0069(4)	0.0140(5)	0.0169(5)	0.0000	0.0020(4)	0.0000
T	Si^{4+}	0.57393(14)	0.16714(10)	0.22369(9)	0.0110	0.1900(10)	0.0086(3)	0.0089(3)	0.0154(4)	–0.0002(4)	0.0021(3)	–0.0003(3)
	Si	0.57393(14)	0.16714(10)	0.22369(9)	0.0110	0.8001(10)	0.0086(3)	0.0089(3)	0.0154(4)	–0.0002(4)	0.0021(3)	–0.0003(3)
O1	O,O^{2-}	0.8267(4)	0.2274(3)	0.1661(3)	0.0204	1	0.0170(10)	0.0248(13)	0.0203(12)	–0.0026(11)	0.0052(9)	–0.0067(10)
O2	O,O^{2-}	0.5093(7)	0.0000	0.1675(4)	0.0204	1	0.0283(19)	0.0107(14)	0.0206(18)	0.0000	–0.0001(15)	0.0000
O3	O,O^{2-}	0.6305(4)	0.1687(3)	0.3914(2)	0.0120	1	0.0107(8)	0.0089(8)	0.0165(10)	–0.0002(10)	0.0028(7)	0.0001(9)
O4	O,O^{2-}	0.1334(6)	0.0000	0.4006(4)	0.0132	1	0.0111(14)	0.0128(14)	0.0160(17)	0.0000	0.0032(13)	0.0000
	H	0.098(15)	0.0000	0.316(9)	0.0132	0.7209(10)	0.0111(14)	0.0128(14)	0.0160(17)	0.0000	0.0032(13)	0.0000

in Redhammer and Roth (2002)]. This indicates that substitution occurs at the O4 hydroxyl site. The shortening of the *c* parameter is partly due to OH ↔ F substitution (Boukili et al. 2001), but it has been shown that substitutions involving a deprotonation mechanism generally play a major role (Cesare et al. 2003; Scordari et al. 2006 and references therein). In particular, it is recognized that Ti-oxy substitutions lead to diagnostic values for some structural features, such as (1) shortening of the *c*-parameter as well as of the K-O4 distance; (2) high values of bond length distortions (BLD) for M2, see Table 8; (3) high values of the shift of the M2 cation from the geometric center of the octahedron toward the O4 oxygen; and (4) low values for $\Delta_{K\text{-}O4}$ and t_{int} (Cruciani and Zanazzi 1994; Cesare et al. 2003; Schingaro et al. 2005a; Scordari et al. 2006). In addition, the occurrence of $M^{3+,4+}$-oxy type substitutions, with $M^{3+,4+} = Al^{3+}$, Fe^{3+}, Ti^{4+}, has been assessed in other Vulture micas (Scordari et al. 2006; Matarrese et al. 2006). In the case of the VUT191 phlogopites, however, not all samples follow the trends typical of oxy-substituted micas (see below).

Individual tetrahedra are regular and slightly elongated in the direction of the $T\text{-}O_{apical}$ bond. The tetrahedral mean bond lengths and parameters describing geometrical features of the tetrahedron (Tables 7, 8, and 10) do not vary much from sample to sample, consistent with the limited compositional variation of the T sites (see Table 9). The examined crystals exhibit an inverse dependence of the α-values relative to their Fe contents, as expected

from comparison to literature data (Cruciani and Zanazzi 1994; Brigatti and Guggenheim 2002; Brigatti et al. 2005). Variations of octahedral bond distances, with <M1-O> in the range 2.074–2.082 Å, and <M2-O> in the range 2.064–2.072 Å (Table 7), and of the octahedral mean atomic numbers (m.a.n.), 14.13 ≤ m.a.n. (M1) ≤ 16.77 e^-, 14.35 ≤ m.a.n. (M2) ≤ 17.04 e^- (Table 10), reflect the variations of the annite component and of the Ti content (see Fig. 1 and accompanying discussion).

The analyzed micas are meso-octahedral from a geometrical viewpoint (Table 7), with the exception of VUT191_1 and VUT191_2 single crystals, which are homo-octahedral (Weiss et al. 1992). From a chemical viewpoint (i.e., considering the mean atomic numbers at the M1 and M2 sites; Table 10), the samples are homo-octahedral (Ďurovíč 1994). Indeed, the average error associated with the refined site-scattering power (here referred to as mean atomic number) is 0.5 e^-, whereas the differences between M1 and M2 mean atomic numbers are within 1 e^- (see Table 10). Systematic differences in structural parameters between samples VUT191_1 and VUT191_2 on the one hand and the remaining single crystals on the other, are apparent from the analyses reported in Tables 7 and 8. They are relevant to the $<K\text{-}O>_{outer}$ (Table 7), t_{int}, $shift_{M2}$ (Table 8) parameters and are probably related to the different Ti and Fe^{3+} substitutions affecting the two groups of samples, as well as to the different degrees of hydrogenation of the two groups of samples (see next section for further details).

Crystal chemistry

Figure 3 illustrates the variation of the *c*-parameter of the micas as a function of the water content as determined by SIMS. It is apparent that micas with the shortest *c*-parameter are more dehydrogenated. However, micas with intermediate *c* values may have remarkably different degrees of dehydrogenation. Inspection of Figures 4 and 5, which plot the out-of-center-shift parameters and the $<K\text{-}O>_{outer}$ distances, respectively, vs. Ti content, show clearly that the samples can be divided into two distinct groups (see section Structural features) that are expected to be affected by different substitution mechanisms. This was confirmed by the comparison of the relevant crystal chemical formulae (Table 9), whose calculation is detailed below.

The crystal-chemical formulae reported on Table 3 were obtained by combining electron microprobe, SIMS, and Mössbauer investigations, using the 12(O, OH, Cl, F) basis. When SIMS analyses where not available, the C-H-N value was used. However, the latter is an average value (see section Micas analyses) and proved not to be suitable for every single crystal, in particular for those characterized by low *c*-values. In the latter cases, indeed, micas should be more strongly dehydrogenated, and the average C-H-N value invariably leads to an overestimation of octahedral vacancies, providing unacceptable discrepancies (in the range 3–5 e^-) between EPMA- and SCXRD-derived mean atomic numbers. In those cases, the OH contents were estimated from structural parameters (*c*, $<K\text{-}O>_{outer}$, see Cruciani and Zanazzi 1994; Cesare et al. 2003), also taking into account the contribution of F to the shortening of the *c*-parameter as well

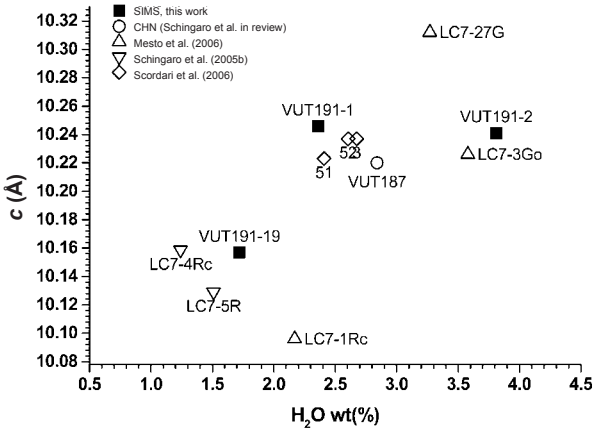

FIGURE 3. A plot of the crystallographic *c* parameter vs. H_2O content. Unless explicitly stated, H_2O (data) are from SIMS measurements.

TABLE 7. Results of structure refinement in space group *C*2/*m*: selected bond distances (Å)

Samples	VUT191_1	VUT191_2	VUT191_10	VUT191_11	VUT191_13	VUT191_19
T-O(1)	1.662(3)	1.663(3)	1.660(2)	1.660(2)	1.661(2)	1.657(2)
T-O(1′)	1.664(3)	1.664(3)	1.665(2)	1.662(2)	1.662(2)	1.662(2)
T-O(2)	1.661(2)	1.663(2)	1.663(1)	1.666(2)	1.660(1)	1.661(2)
T-O(3)	1.656(3)	1.664(3)	1.675 (1)	1.679(2)	1.677(2)	1.677(3)
<T-O>	1.661	1.664	1.666	1.667	1.665	1.664
M1-O(4)(×2)	2.050(4)	2.037(5)	2.047(2)	2.042(3)	2.043(3)	2.038(4)
M1-O(3)(×4)	2.094(3)	2.092(3)	2.098 (2)	2.097(2)	2.102(2)	2.097(2)
<M1-O>	2.079	2.074	2.081	2.079	2.082	2.077
M2-O(4)(×2)	2.034(3)	2.021(4)	2.010(2)	1.999(3)	1.986(2)	1.983(3)
M2-O(3)(×2)	2.088(3)	2.087(3)	2.086(1)	2.084(2)	2.085(2)	2.086(2)
M2-O(3′)(×2)	2.094(3)	2.098(3)	2.110(2)	2.116(3)	2.122(2)	2.123(3)
<M2-O>	2.072	2.069	2.069	2.066	2.064	2.064
<M-O>	2.074	2.071	2.073	2.070	2.070	2.068
K-O(1)(×4)	2.947(3)	2.939(3)	2.944(2)	2.942(2)	2.945(2)	2.943(3)
K-O(1′)(×4)	3.386(3)	3.392(3)	3.364(2)	3.355(2)	3.343(2)	3.346(3)
K-O(2)(×2)	2.948(5)	2.939(5)	2.948(2)	2.941(3)	2.949(3)	2.943(4)
K-O(2′)(×2)	3.396(4)	3.398(5)	3.374(2)	3.368(3)	3.361(3)	3.362(4)
$<K\text{-}O>_{inner}$	2.947	2.939	2.945	2.942	2.946	2.943
$<K\text{-}O>_{outer}$	3.389	3.394	3.367	3.359	3.349	3.351
<K-O>	3.169	3.167	3.156	3.151	3.148	3.147

TABLE 8. Selected distortional parameters derived from the structure refinements in space group *C2/m*

	VUT 191_1	VUT 191_2	VUT 191_10	VUT 191_11	VUT 191_13	VUT 191_19
t_{tet} (Å)	2.231	2.239	2.247	2.254	2.250	2.249
BLD_T	0.142	0.030	0.252	0.356	0.342	0.387
$Volume_T$ (Å^3)	2.349	2.361	2.370	2.376	2.368	2.365
TQE	1.000	1.000	1.000	1.000	1.000	1.000
TAV	0.972	0.880	0.789	0.963	0.908	0.760
τ (°)	110.257	110.208	110.159	110.253	110.218	110.133
α (°)	9.63	10.02	9.24	9.09	8.74	8.90
Δz (Å)	0.008	0.004	0.012	0.011	0.019	0.014
D.M. (Å)	0.555	0.582	0.571	0.576	0.569	0.576
ψ_{M1} (°)	58.91	59.09	59.28	59.38	59.46	59.47
ψ_{M2} (°)	58.79	59.02	59.08	59.18	59.17	59.24
BLD_{M1}	0.942	1.164	1.087	1.179	1.264	1.268
ELD_{M1}	5.024	5.235	5.452	5.567	5.663	5.668
BLD_{M2}	1.206	1.549	1.885	2.156	2.527	2.614
ELD_{M2}	4.879	5.137	5.207	5.323	5.301	5.390
$Shift_{M2}$ (Å)	0.012	0.025	0.044	0.055	0.068	0.072
$Volume_{M1}$ (Å^3)	11.800	11.671	11.783	11.732	11.790	11.703
OQE_{M1}	1.011	1.012	1.013	1.014	1.014	1.014
OAV_{M1}	36.557	39.593	42.743	44.565	46.108	46.117
$Volume_{M2}$ (Å^3)	11.680	11.597	11.592	11.542	11.506	11.486
OQE_{M2}	1.011	1.012	1.013	1.013	1.014	1.014
OAV_{M2}	34.814	38.826	40.299	42.600	43.216	44.844
$e_u(M1)/e_s(M1)$	1.106	1.111	1.115	1.118	1.120	1.120
$e_u(M2)/e_s(M2)$	1.103	1.108	1.110	1.112	1.112	1.114
t_{oct} (Å)	2.147	2.130	2.126	2.117	2.116	2.111
t_{int} (Å)	3.424	3.415	3.360	3.339	3.329	3.332
$\Delta_{K\text{-}O4}$ (Å)	0.442	0.455	0.422	0.417	0.403	0.408
$t_{K\text{-}O4}$ (Å)	3.967	3.978	3.948	3.948	3.945	3.944

Notes: t_{tet} = tetrahedral sheet thickness calculated from z coordinates of basal and apical O atoms; TQE = tetrahedral quadratic elongation (Robinson et al. 1971); TAV = tetrahedral angle variance (Robinson et al. 1971); τ = tetrahedral flattening angle; α = tetrahedral rotation angle (Hazen and Burnham. 1973); Δz = departure from co-planarity of the basal O atoms (Güven 1971); D.M. = dimensional misfit between tetrahedral and octahedral sheets (Toraya. 1981); ψ = octahedral flattening angles (Donnay et al. 1964); BLD = bond-length distortions (Renner and Lehmann 1986); ELD = edge-length distortion (Renner and Lehman. 1986); $Shift_{M2}$ = off-center shift of the M2 cation defined as the distance between the refined position of cation and the geometrical center of M2 site (coordinates: x/a = 0.0, y/b = 0.8333, z/c = 0.5); OQE = octahedral quadratic elongation (Robinson et al. 1971); OAV = octahedral angle variance (Robinson et al. 1971); eu, es = mean lengths of unshared and shared edges (Toraya,1981), respectively; t_{oct} = octahedral sheet thickness (Toraya, 1981); t_{int} calculated from the z coordinates of basal O atoms; $\Delta_{K\text{-}O4} = \langle K\text{-}O\rangle_{outer} - \langle K\text{-}O\rangle_{inner}$; $t_{K\text{-}O4}$ = projection of K-O4 distance along c*.

TABLE 9. Final crystal chemical formulae for VUT191 phlogopite

VUT191_1	$(K_{0.78}Na_{0.09}Ba_{0.03}\square_{0.10})(Al_{0.14}Mg_{2.19}\ Fe^{2+}_{0.10}Fe^{3+}_{0.30}Ti_{0.13}Cr_{0.02}\square_{0.12})(Si_{2.68}Al_{1.32})O_{10.06}F_{0.10}OH_{1.84}$
VUT191_2	$(K_{0.82}Na_{0.09}Ba_{0.03}\square_{0.06})(Al_{0.12}Mg_{2.11}Fe^{2+}_{0.11}Fe^{3+}_{0.31}Ti_{0.15}\ Cr_{0.01}\square_{0.19})(Si_{2.72}Al_{1.28})O_{10}F_{0.15}OH_{1.86}$
VUT191_10	$(K_{0.81}Na_{0.09}Ba_{0.07}\square_{0.03})(Al_{0.08}Mg_{1.81}Mn_{0.01}Fe^{2+}_{0.19}Fe^{3+}_{0.56}Ti_{0.27}\square_{0.08})(Si_{2.62}Al_{1.38})O_{10.69}F_{0.15}Cl_{0.01}OH_{1.15}$
VUT191_11	$(K_{0.78}Na_{0.09}Ba_{0.09}\square_{0.04})(Al_{0.13}Mg_{1.73}Mn_{0.01}Fe^{2+}_{0.20}Fe^{3+}_{0.57}Ti_{0.28}\square_{0.08})(Si_{2.67}Al_{1.33})O_{10.78}F_{0.24}Cl_{0.01}OH_{0.97}$
VUT191_13	$(K_{0.77}Na_{0.09}Ba_{0.08}\square_{0.06})(Al_{0.19}Mg_{1.69}\ Fe^{2+}_{0.19}Fe^{3+}_{0.56}Ti_{0.27}\square_{0.10})(Si_{2.71}Al_{1.29})O_{10.79}F_{0.22}Cl_{0.01}OH_{0.98}$
VUT191_19	$(K_{0.78}Na_{0.09}Ba_{0.09}\square_{0.04})(Al_{0.11}Mg_{1.70}Mn_{0.01}Fe^{2+}_{0.20}Fe^{3+}_{0.59}Ti_{0.30}Li_{0.01}\square_{0.08})(Si_{2.66}Al_{1.34})O_{10.79}F_{0.31}Cl_{0.01}OH_{0.89}$

TABLE 10. Mean atomic numbers (e^-) of cation sites and octahedral and tetrahedral mean distances (Å), as determined from structure refinement (X-ref) and chemical analyses (EPMA) (see text for details)

	VUT191_1	VUT191_2	VUT191_10	VUT191_11	VUT191_13	VUT191_19
M1 $e^-_{X\text{-}ref}$	14.15	14.13	16.77	16.35	16.10	15.99
M2 $e^-_{X\text{-}ref}$	14.35	14.65	17.00	16.96	17.04	16.95
(M1+2M2) $e^-_{X\text{-}ref}$	42.85	43.43	50.77	50.27	50.18	49.89
(M1+2M2) e^-_{EMPA}	41.90	41.34	48.45	48.88	48.06	49.25
K $e^-_{X\text{-}ref}$	19.09	19.36	21.07	21.31	21.45	21.44
K e^-_{EMPA}	17.49	18.25	20.30	20.85	20.10	20.85
T $e^-_{X\text{-}ref}$	13.86	13.95	13.90	13.91	13.90	13.86
T e^-_{EMPA}	13.68	13.68	13.66	13.67	13.68	13.67
$\langle T\text{-}O\rangle_{X\text{-}ref}$	1.661	1.664	1.666	1.667	1.665	1.664
$\langle T\text{-}O\rangle_{EMPA}$	1.667	1.667	1.670	1.668	1.667	1.669
$\langle M\text{-}O\rangle_{X\text{-}ref}$	2.074	2.071	2.073	2.070	2.070	2.068
$\langle M\text{-}O\rangle_{EMPA}$	2.072	2.075	2.061	2.061	2.058	2.060

as charge-balance considerations. The final crystal-chemical formulae are compiled in Table 9.

For sample VUT191-1, the average water content provided by C-H-N analysis was initially used for the formula recalculation (see Table 3). This value gave a sum of octahedral cations greater than 3 apfu. Considering the close similarity of this sample to sample VUT191_2, both with respect to chemistry (Fe/Mg, Ti content) and structural features (Tables 7 and 8 and Figs. 4 and 5), it was concluded that the water contents of these two samples should also be similar. As a result, the final formula listed in Table 9 for VUT191_1 was calculated using the same water content as sample VUT191_2. For VUT191_2 and VUT191_19 (i.e., for samples for which SIMS data were available), the formulae in Tables 3 and 9 coincide.

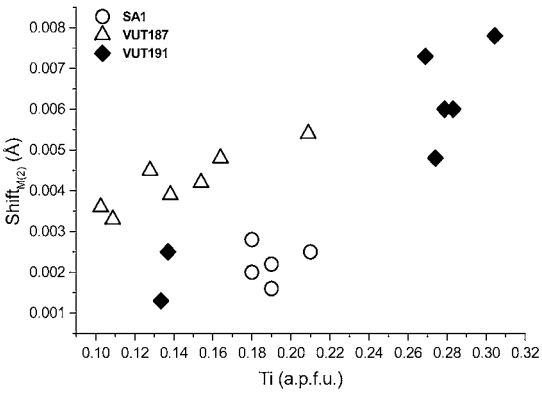

FIGURE 4. A plot of the parameter shift$_{M2}$ vs. Ti content. High values of the shift$_{M2}$ parameter are associated with the occurrence of Ti-oxy substitutions. VUT191 phlogopite samples (filled diamond) plot in two separate groups (see text). SA1 and VUT 187 samples references as in Figure 1.

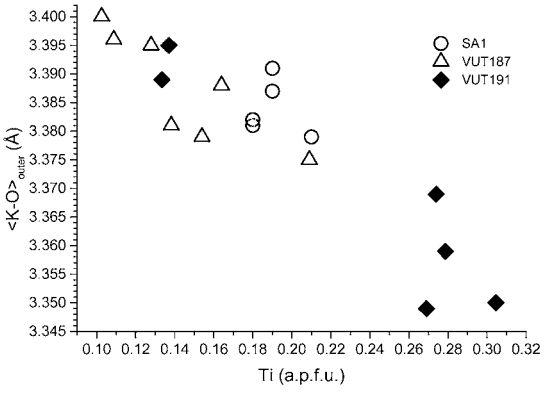

FIGURE 5. A plot of the parameter <K-O>$_{outer}$ vs. Ti content. The decrease of <K-O>$_{outer}$ distance as a function of the Ti content is associated with an increase in the amount of the oxy-component. VUT191 phlogopite samples (filled diamonds) plot in two separate groups (see text). SA1 and VUT 187 samples references as in Figure 1.

For samples from VUT191_10 to VUT191_19 in Table 9, apart from the M^{3+}-Tschermak substitutions ($^{VI}M^{2+} + {}^{IV}Si^{4+} \leftrightarrow {}^{VI}M^{3+} + {}^{IV}Al^{3+}$, with M^{3+} = Al, Fe^{3+}), the remaining M^{3+} cations and the Ti^{4+} cations are involved in M^{3+}-oxy [$^{VI}M^{2+} + (OH)^- \leftrightarrow M^{3+} + O^{2-} + ½H_2$] and Ti-oxy substitutions [$^{VI}M^{2+} + 2(OH)^- \leftrightarrow {}^{VI}Ti^{4+} + 2O^{2-} + H_2$], respectively. Low concentrations of octahedral vacancies are present and are charge-balanced through the Ti-vacancy substitution ($2\ {}^{VI}M^{2+} \leftrightarrow {}^{VI}Ti^{4+} + {}^{VI}\square$).

Samples VUT191_1 and VUT191_2 instead have negligible or no oxy component. Sample VUT191_1 contains a high concentration of octahedral vacancies that are balanced through the Ti-vacancy mechanism. In sample VUT191_2, both Ti-vacancy and the dioctahedral-trioctahedral ($3\ {}^{VI}M^{2+} \leftrightarrow 2\ {}^{VI}M^{3+} + {}^{VI}\square$ mechanism seem to be active.

The formulae in Table 9 generally demonstrate good agreement between observed and calculated mean atomic numbers, as well as between observed octahedral average bond distances and those calculated from the chemical molar fraction and atomic radii in Shannon (1976). In all the Fe- and Ti-rich samples (see Table 10, from sample VUT191_10 to VUT191_19), a tendency toward a systematic underestimation of the average octahedral bond distances is apparent. Such systematic variations of the observed bond lengths with respect to the radii of Shannon (1976) are already known (Bailey 1984; Gibbs et al. 1997; Mercier et al. 2006). In particular, Mercier et al. (2006) observed that for non end-member single-crystal biotite-1*M* structure, bond lengths calculated from Shannon's radii tend to overestimate octahedral mean bond lengths between the Fe^{2+} and Mg^{2+} end-member, whereas the opposite is true when substitution by smaller +3, +4 cations occurs. Our data are consistent with those findings. Unfortunately, the new cation and coordination-specific bond lengths that these authors provided, apart from not being complete, are more suitable for trioctahedral micas with simpler compositions close to the M^{2+}-end members.

Another explanation for the discrepancies in observed vs. calculated average octahedral bond lengths in our samples is that the Fe^{2+}/Fe^{3+} ratio provided by Mössbauer spectroscopy could be an "average" value, so that single crystals might depart from this value to different extents.

FURTHER REMARKS

Petrographic and chemical evidence for VUT191 phlogopite shows a complete range of composition originating close to mantle micas and progressing up to high-*T*/low-*P* subvolcanic micas. This variation indicates that micas can be passed through different stages of magmatic evolution, starting from a foiditic (nephelinitic) and/or melilititic primary magma, to a tephri-foiditic, and then to a thepri-fonolitic term.

Chemical and structural data revealed that VUT191 phlogopite clusters into two groups, each characterized by different H contents and different Ti substitutions, in particular $^{VI}M^{2+} + 2(OH)^- \leftrightarrow {}^{VI}Ti^{4+} + 2O^{2-} + H_2$ (Ti-oxy) and $^{VI}M^{2+} \leftrightarrow {}^{VI}Ti^{4+} + {}^{VI}\square$ (Ti-vacancy). This is a crucial point because the assessment of correct substitution mechanisms in biotite not only clarifies the behavior of petrologically interesting species (such as Fe, Ti) when they are incorporated into the mica structure, but also affects the choice of the annite activity model from which several petrogenetic parameters may be derived (see for instance Fabbrizio et al. 2006).

Finally, Mössbauer results of the phlogopite analyzed here, as well as those analyzed in previous works (Matarrese et al. 2005; Scordari et al. 2006; Matarrese 2007) suggest variable f_{O_2} and f_{H_2O} during the crystallization of micas of intermediate Monte Vulture pyroclastics. Thus, crystal settling of mafic minerals cannot account entirely for magma differentiation. Variable phreatomagmatic phenomena could help to explain not only such broad variations but also slightly different evolution patterns for the primary foiditic, melilititic melt.

Mica chemistry and structure can be used to predict bulk-rock chemistry, with the latter being modified by abundant analcime (plus cancrinite) formation during late-magmatic stages (Stoppa et al. 2006). The evolutionary stages experienced by the micas (see above) could parallel a possible polybaric/polythermal evolution from melilititic, nephelinitic, and phonolitic-foidite

to phonolite, which is more commonly observed at Mt. Vulture. According to a previous hypothesis, all rock types of the Vulture may derive from two rock series, one melilite-bearing and one melilite-free (Melluso et al. 1996). However, melilite-bearing series share the same geological setting as melilite-free series and occur together, with melilite-bearing and melilite-free rocks being persistently similar in petrochemistry and geochemistry (e.g., isotopes). Trace-element distributions in carbonatites/melilitites and foidites are also very similar. These features are difficult to reconcile with a hypothesis of two distinct parental magmas. Open-system crystallization conditions and variable H_2O/CO_2 may have affected the composition of the primary magma found in melt inclusions in olivine, clinopyroxene, and apatite from the Vulture phonolitic foidite (Sololova et al. 2005).

The combination of analytical methods used in the present paper has shown that volcanic micas are able to provide information related to their geological history even in complex cases such as those considered here, where the micas are characterized by notable chemical variability. However, other than complete chemical and structural analysis, the use of single-crystal techniques, both for hydrogen determinations (such as SIMS) and for Fe speciation (such as micro-XANES or other element-sensitive techniques) could help to shed light into the uncertainties related to the results of the bulk analytical methods.

ACKNOWLEDGMENTS

The authors are grateful to Marcello Serracino for assistance during electron probe microanalyses at the Istituto di Geologia Ambientale e Geoingegneria, CNR, Rome. Antonio Giaretta is thanked for C-H-N measurements at CNR-IGC, Padova. Detailed reviews by G. Redhammer and an anonymous reviewer greatly improved the final manuscript. This work was supported by the COFIN-MIUR.

REFERENCES CITED

Alietti, E., Brigatti, M.F., and Poppi, L. (1995) The crystal structure and chemistry of high-aluminum phlogopite. Mineralogical Magazine, 59, 149–157.

Bailey, S.W. (1984) Micas, 13, 584 p. Reviews in Mineralogy and Geochemistry, Mineralogical Society of America, Chantilly, Virginia.

Betteridge, P.W., Carruthers, J.R., Copper, R.I., Prouth, K., and Watkin, D.J. (2003) Crystals version 12: Software for guided crystal structure analysis. Journal of Applied Crystallography, 36, 1487–1492.

Bohlen, S.R., Peacor, D.R., and Essene, E.J. (1980) Crystal chemistry of a metamorphic biotite and its significance in water barometry. American Mineralogist, 65, 55–62.

Boukili, B., Robert, J.L., Beny, J.M., and Holtz, F. (2001) Structural effects of OH → F substitution in trioctahedral micas of the system: K_2O-FeO-Fe_2O_3-Al_2O_3-SiO_2-H_2O-HF. Schweizerische Mineralogische und Petrographische Mitteilungen, 81, 55–67.

Brigatti, M.F. and Guggenheim, S. (2002) Mica crystal chemistry and the influence of pressure, temperature, and solid solution on atomistic models. In A. Mottana, F.P. Sassi, J.B. Thompson, and S. Guggenheim, Eds., Micas: Crystal Chemistry and Metamorphic Petrology, 46, p. 1–100. Reviews in Mineralogy and Geochemistry, Mineralogical Society of America, Chantilly, Virginia.

Brigatti, M.F., Caprilli, E., Funiciello, R., Giordano, G., Mottana, A., and Poppi, L. (2005) Crystal chemistry of ferroan phlogopites from the Albano maar lake zone (Colli Albani volcano, central Italy). European Journal of Mineralogy, 17, 611–621.

Brocchini, D., La Volpe, L., Laurenzi, M.A., and Principe, C. (1994) Storia evolutiva del Monte Vulture. Plinius, 12, 22–25.

Bruker (2003a) SAINT. Bruker AXS Inc., Madison, Wisconsin.

——— (2003b) APEX2. Bruker AXS Inc., Madison, Wisconsin.

Cesare, B., Cruciani, G., and Russo, U. (2003) Hydrogen deficiency in Ti-rich biotite from anatectic metapelites (El Joyazo, SE Spain): Crystal-chemical aspects and implications for high-temperature petrogenesis. American Mineralogist, 88, 583–595.

Chakhmouradian, A.R. (2006) High-field-strength elements in carbonatitic rocks: Geochemistry, crystal chemistry and significance for constraining the sources of carbonatites. Chemical Geology, 235, 138–160.

Cruciani, G. and Zanazzi, P.F. (1994) Cation partitioning and substitution mechanism in 1*M* phlogopite: A crystal chemical study. American Mineralogist, 79, 289–301.

De La Roche, H., Leterrier, J., Grande, C.P., and Marchal, M. (1980) A classification of volcanic and plutonic rocks using R1-R2 diagrams and major elements analyses: Its relationship and current nomenclature. Chemical Geology, 29, 183–210.

Donnay, G., Morimoto, N., Takeda, H., and Donnay, J.D.H. (1964a) Trioctahedral one-layer micas. I. Crystal structure of a synthetic iron mica. Acta Crystallographica, 17, 1369–1373.

Donnay, G., Donnay, J.D.H., and Takeda, H. (1964b) Trioctahedral one-layer micas. II Prediction of the structure from composition and cell dimensions. Acta Crystallographica, 17, 1374–1381.

Ďurovíč, S. (1994) Classification of phyllosilicates according to the symmetry of their octahedral sheets. Ceramics—Silikàty, 38, 81–84.

Dyar, M.D. (2002) Optical and Mössbauer spectroscopy of iron in micas. In A. Mottana, F.P. Sassi, J.B. Thompson, and S. Guggenheim, Eds., Micas: Crystal Chemistry and Metamorphic Petrology, 46, p. 313–340. Reviews in Mineralogy and Geochemistry, Mineralogical Society of America, Chantilly, Virginia.

Fabbrizio, A., Rouse, J.P., and Carroll, M.R. (2006) New experimental data on biotite+magnetite+sanidine saturated phonolitic melts and application to the estimation of magmatic water fugacity. American Mineralogist, 91, 1863–1870.

Feldstein, S.N., Lang, R.A., Vennemann, T., and O'Neil, J.R. (1996) Ferric-ferrous ratios, H_2O contents and D/H ratios of phlogopite and biotite from lavas of different tectonic regimes. Contributions to Mineralogy and Petrology, 126, 51–66.

Forbes, W.C. and Flower, M.F.J. (1974) Phase relations of titan-phlogopite, $K_2Mg_4TiAl_2Si_6O_{20}(OH)_4$: a refractory in the upper mantle? Earth and Planetary Science Letters, 22, 60–66.

Giannandrea, P., La Volpe, L., Principe, C., and Schiattarella, M. (2006) Unità stratigrafiche a limiti inconformi e storia evolutiva del vulcano medio-pleistocenico del Monte Vulture (Appennino Meridionale, Italia). Bollettino della Societa' Geologica Italiana, 125, 67–92.

Gibbs, G.V., Tamada, O., and Boisen, Jr., M.B. (1997) Atomic and ionic radii: a comparison with radii derived from electron density distributions. Physics and Chemistry of Minerals, 24, 432–439.

Güven, N. (1971) The crystal structure of $2M_1$ phengite and $2M_1$ muscovite. Zeischrift für Kristallographie, 134, 196–212.

Hawthorne, F.C., Ungaretti, L., and Oberti, R. (1995) Site populations in minerals: terminology and presentation of results. Canadian Mineralogist, 33, 907–911.

Hazen, R.M. and Burnham, C.W. (1973) The crystal structure of one layer phlogopite and annite. American Mineralogist, 58, 889–900.

Henry, D.J. and Guidotti, C.V. (2002) Titanium in biotite from metapelitic rocks: Temperature effects, crystal-chemical controls, and petrologic applications. American Mineralogist, 87, 375–382.

Henry, D.J., Guidotti, C.V., and Thompson, J. (2005) The Ti-saturation surface for low-to-medium pressure metapelitic biotites: implications for geothermometry and Ti-substitution mechanisms. American Mineralogist, 90, 316–328.

Irvine, T.N. and Bargar, W.R.A. (1971) A guide to the chemical classification of the common volcanic rocks. Canadian Journal of Earth Science, 8, 523–548.

Lagarec, K. and Rancourt, D.G. (1997) Extended Voigt-based analytic lineshape method for determining N-dimensional correlated hyperfine parameter distributions in Mössbauer spectroscopy. Nuclear Instruments and Methods in Physics Research, B129, 266–280.

——— (1998) RECOIL. Mössbauer spectral analysis software. University of Ottawa, Canada (www.isapps.ca/recoil).

Matarrese, S. (2007). Cristallochimica comparativa di flogopiti del Monte Vulture, 170 p. Ph.D. thesis, University of Bari, Italy.

Matarrese, S., Mesto, E., Pedrazzi, G., Schingaro, E., and Scordari, F. (2005) Trioctahedral micas from the youngest volcanics of Mt. Vulture (Pz, Italy): a Crystal chemical study. International workshop Micas@Italy, Rimini(Italy), February 9–11, 2005, Book of Abstract, 33.

Matarrese, S., Schingaro E., Scordari, F., Rosatelli, G., Stoppa, F., and Pedrazzi, G. (2006) Micas as indicators of geological processes: The case of Mt. Vulture (Italy). Annual meeting of the Geological Society of America, Philadelphia, 22–25 October 2006. Geological Society of America, Abstracts with Programs, Vol. 38, No. 7, p. 292.

Melluso, L., Morra, V., and Di Girolamo, P. (1996) The Mt. Vulture volcanic complex (Italy): Evidence for distinct parental magmas and for residual melts wirh melilite. Mineralogy and Petrology, 56, 225–250.

Mercier, P.H.J., Rancourt, D.G., Redhammer, G.J., Lalonde, A.E., Robert, J-L., Berman, R.G., and Kodama, H. (2006) Upper limit of tetrahedral rotation angle and factors affecting octahedral flattening in synthetic and natural 1*M* polytype *C*2/*m* space group micas. American Mineralogist, 91, 831–849.

Mesto, E., Schingaro, E., Scordari, F., and Ottolini, L. (2006) Electron probe microanalysis, secondary ion mass spectrometry and single crystal X-ray diffraction study of phlogopites from Mt. Vulture, Potenza, Italy: Consideration of cation partitioning. American Mineralogist, 91, 182–190.

Nespolo, M. and Ferraris, G. (2001) Effects of the stacking faults on the calculated

electron density of mica polytypes—The Ďurovíč effect. European Journal of Mineralogy, 13, 1035–1045.
Ottolini, L. and Hawthorne, F.C. (2001) SIMS ionization of hydrogen in silicates: a case study of kornerupine. Journal of Analytical Atomic Spectrometry, *6*, 1266–1270.
Ottolini, L., Bottazzi, P., and Vannucci, R. (1993) Quantification of lithium, beryllium and boron in silicates by secondary ion mass spectrometry using conventional energy filtering. Analytical Chemistry, 65, 1960–1968.
Ottolini, L., Bottazzi, P., Zanetti, A., and Vannucci, R. (1995) Determination of hydrogen in silicates by secondary ion mass spectrometry. Analyst, 120, 1309–1313.
Ottolini, L., Camara, F., Hawthorne, F.C., and Stirling, J. (2002) SIMS matrix effects in the analysis of light elements in silicate minerals: Comparison with SREF and EMPA data. American Mineralogist, 87, 1477–1485.
Pouchou, J.L. and Pichoir, F. (1985) 'PAP' $\Phi(\rho Z)$ procedure for improved quantitative micro-analysis. Microbeam Analysis, 104–160.
Rancourt, D.G. and Ping, J.Y. (1991) Voigt-based methods for arbitrary-shape static hyperfine parameter distribution in Mössbauer spectroscopy. Nuclear Instruments and Methods in Physics Research, B58, 85–97.
Rancourt, D.G., Tume, P., and Lalonde, A.E. (1993) Kinetics of the $(Fe^{2+}OH)_{mica} \rightarrow (Fe^{3+}O^{2-})_{mica} + H$ oxidation reaction in bulk single crystal biotite studied by Mössbauer spectroscopy. Physics and Chemistry of Minerals, 20, 276–284.
Rancourt, D.C., Christie, I.A.D., Royer M., Kodama, H., Robert, J.-L., Lalonde, A.E., and Murad, E. (1994a) Determination of accurate $^{4}Fe^{3+}$, $^{6}Fe^{3+}$, and $^{6}Fe^{2+}$ site populations in synthetic annite by Mössbauer spectroscopy. American Mineralogist, 79, 51–62.
Rancourt, D.G., Ping, J.Y., and Berman, R.G. (1994b) Mössbauer Spectroscopy of Minerals III. Octahedral-site Fe^{2+} quadrupole splitting distributions in the phlogopite-annite series. Physics and Chemistry of Minerals, 21, 258–267.
Redhammer, G.J. (1998) Characterization of synthetic trioctahedral micas by Mössbauer spectroscopy. Hyperfine Interactions, 117, 85–115.
Redhammer, G.J. and Roth, G. (2002) Single-crystal structure refinements and crystal chemistry of synthetic trioctahedral micas $KM_3(Al^{3+}, Si^{4+})_4O_{10}(OH)_2$, where $M = Ni^{2+}$, Mg^{2+}, Co^{2+}, Fe^{2+}, or Al^{3+}. American Mineralogist, 87, 1464–1476.
Redhammer, G.J., Amthauer, G., Lottermoser, W., Bernroider, M., Tippelt, G., and Roth, G. (2005) X-ray powder diffraction and ^{57}Fe-Mössbauer spectroscopy of synthetic trioctahedral micas $\{K\}(Me_3)<TSi_3>O_{10}(OH)_2$, $Me = Ni^{2+}$, Mg^{2+}, Co^{2+}, Fe^{2+}; $T = Al^{3+}$, Fe^{3+}. Mineralogy and Petrology, 85, 89–115.
Renner, B. and Lehmann, G. (1986) Correlation of angular and bond length distortions in TO_4 units in crystals. Zeitschrift für Kristallographie, 175, 43–59.
Righter, K., Dyar, M.D., Delaney, J.S., Vennemann, T.W., Hervig, R.L., and King, P.L. (2002) Correlations of octahedral cations with OH, O^2, Cl, and F in biotite from volcanic rocks and xenoliths. American Mineralogist, 87, 142–153.
Robert, J.L. (1976) Titanium solubility in synthetic phlogopite solid solution. Chemical Geology, 17, 213–227.
Robinson, K., Gibbs, G.V., and Ribbe, P.H. (1971) Quadratic elongation, a quantitative measure of distortion in coordination polyhedra. Science, 172, 567–570.
Salvador, A. (1987) Unconformity-bounded stratigraphic units. Geological Society of American Bulletin, 98, 232–237.
Schingaro, E., Scordari, F., and Ventruti, G. (2001) Trioctahedral micas-1*M* from Mt. Vulture (Italy): Structural disorder and crystal chemistry. European Journal of Mineralogy, 13, 1057–1069.
Schingaro, E., Scordari, F., Mesto, E., Brigatti, M.F., and Pedrazzi, G. (2005a) Cation site partitioning in Ti-rich micas from Black Hill (Australia): A multitechnical approach. Clays and Clay Minerals, 53, 179–189.
Schingaro, E., Scordari, F., and Ottolini, L. (2005b) Ti and Fe rich phlogopites from Mt. Vulture (Potenza, Italy): A combined EPMA, SIMS and SCXRD study. GEOITALIA 2005, Spoleto (Italy), September 21–23, 2005, EPITOME, 61.
Schingaro, E., Scordari, F., Matarrese, S., Stoppa, F., Rosatelli, G., and Pedrazzi, G. (2006) Trioctahedral micas from Mt. Vulture (Potenza, Italy): chemical and structural trends. XXXV AIC meeting, Ferrara, september 18–21, 2006. Collected Abstracts, MS1-O3.
Scordari, F., Ventruti, G., Sabato, A., Bellatreccia, F., Della Ventura, G., and Pedrazzi, G. (2006) Ti-rich phlogopite from Monte Vulture (Potenza, Italy) investigated by a multianalytical approach: Substitutional mechanisms and orientation of the OH dipoles. European Journal of Mineralogy, 18, 379–391.
Shabani, A.A.T. (1999) Mineral Chemistry and Mössbauer Spectroscopy of Micas from Granitic Rocks of the Canadian Appalachians. Ph.D. thesis, University of Ottawa, Canada.
Shannon, R.D. (1976) Revised effective ionic radii and systematic studies of interatomic distances in halides and chalcogenides. Acta Crystallographica, A32, 751–767.
Sheldrick, G.M. (2003) SADABS, Program for empirical absorption correction of area detector data. University of Göttingen, Germany.
Sololova, I.P., Girnis, A.V., Kogarko, L.N., Kononkova, N.N., Stoppa, F., and Rosatelli, G. (2005) Compositions of magmas and carbonate-silicate liquid immiscibility in the Vulture alkaline igneous complex, Italy. Lithos, Special Issue Eurocarb, 85, 113–128.
Stoppa, F., Rosatelli, G., and Principe, C. (2006) Classificazione modale delle vulcaniti del Monte Vulture. In C. Principe, Ed., La geologia del Monte Vulture, Regione Basilicata, p. 87–103. CNR, Potenza, Italy.
Toraya, H. (1981) Distortions of octahedra and octahedral sheets in 1*M* micas and the relation to their stability. Zeitschrift für Kristallographie, 157, 173–190.
Virgo, D. and Popp, R.K. (2000) Hydrogen deficiency in mantle-derived phlogopites. American Mineralogist, 85, 753–759.
Watkin, D.J. (1994) The control of difficult refinements. Acta Crystallographica, A50, 411–437.
Weiss, Z., Rieder, M., and Chmíelovà, M. (1992) Deformation of coordination polyhedra and their sheets in phyllosilicates. European Journal of Mineralogy, 4, 665–682.

Manuscript received February 1, 2007
Manuscript accepted July 20, 2007
Manuscript handled by Francesco Sassi